



Adjustable active–passive dual-frequency liquid crystal smart window based on thermally responsive chiral molecules

Zheng-Wei Lu^a, Victor Ya. Zyryanov^b, Wei Lee^{c,*}

^a Institute of Photonic System, College of Photonics, National Yang Ming Chiao Tung University, Guiren Dist., Tainan 711010, Taiwan

^b Kirensky Institute of Physics, Federal Research Center “Krasnoyarsk Scientific Center,” Siberian Branch of the Russian Academy of Sciences, Krasnoyarsk 660036, Russia

^c Institute of Imaging and Biomedical Photonics, College of Photonics, National Yang Ming Chiao Tung University, Guiren Dist., Tainan 711010, Taiwan

ARTICLE INFO

Keywords:

Dual-frequency liquid crystal
Crossover frequency
Thermosensitive chiral dopant
Cholesteric liquid crystal
Dichroic dye
Smart window

ABSTRACT

We present a cholesteric liquid crystal (CLC) smart window with both passive and active control mechanisms, capable of reversible thermo-optical switching from high-transmission to low-transmission states as the temperature increases. By incorporating a mixture of a thermoresponsive chiral dopant and a left-handed chiral dopant into dual-frequency liquid crystal (DFLC), we have produced thermosensitive CLC that exhibit weak left-handed chirality at low temperature and enhanced left-handed chirality at rising temperature. This change in chirality strength results in increasing thickness-to-pitch ratio as the ambient temperature increases, transforming the CLC texture from the homeotropic to fingerprint state. Additionally, we doped a dichroic dye into the thermosensitive CLC to promote the contrast ratio between the high-transmission homeotropic and low-transmission fingerprint optical textures. Simultaneously, dielectric anisotropy in the host DFCL at different frequencies allows for adjustable switching temperature and varying transparency level. This advancement in smart window technology offers more control options and holds significant potential for practical applications.

1. Introduction

In recent years, growing awareness of environmental protection has led to a focus on creating sustainable lifestyles. Beyond using ecofriendly products, intelligent living solutions can be adopted as well. Smart windows offer sustainable benefits by responsively adjusting indoor lighting, saving energy, and reducing carbon emissions. They allow users to enjoy beautiful outdoor scenery while providing the most comfortable brightness, making them both environmentally friendly and enhancing the convenience of daily living. Over the past decades, extensive research has been conducted on switchable smart windows, which can be divided, based on their operating mechanisms, into the following categories: electrochromic [1,2], photochromic [3,4], and thermochromic [5,6]. The main types of electrochromic products include suspended particle devices [7–9], polymer-dispersed liquid crystals (PDLC) [10–12], and other electrochromic devices [13–15]. These systems require the regulation of an applied electric field to alter their transmission and are therefore considered of active control. In contrast, photochromic and thermochromic smart windows can automatically adjust their transmission state according to light intensity or

temperature, making these passive devices more environmentally friendly and convenient. Because both the active and passive functions are beneficial, this study introduces a smart window designed with dual control mechanisms: both electrically active and thermally passive regulation.

Liquid crystal (LC) substances are widely used in smart windows due to their electrically controllable anisotropic properties including birefringence [16]. A key aspect of photochromic smart windows is the incorporation of photosensitive materials such as azobenzene molecules [17]. These molecules rearrange the LC molecules when exposed to different wavelengths λ of light and alter the central wavelength of the cholesteric LC (CLC) Bragg reflective band through their reversible *trans-cis* isomerization, thereby adjusting transmittance or color [18–20]. While the smectic–CLC phase transition of PDLC is common in the working of thermochromic smart windows [21–23], the switching temperature cannot be modified because of its fixed phase transition point, and the polymeric component in PDLC also significantly increases the required operating voltage. Liang et al. reported a system combining PDLC and polymer-stabilized LC using tungsten-doped vanadium dioxide (W-VO₂) nanocrystals sandwiched between two pieces of

* Corresponding author.

E-mail address: Wei.Lee@nycu.edu.tw (W. Lee).

<https://doi.org/10.1016/j.molliq.2024.126383>

Received 13 July 2024; Received in revised form 26 September 2024; Accepted 28 October 2024

Available online 31 October 2024

0167-7322/© 2024 Elsevier B.V. All rights reserved, including those for text and data mining, AI training, and similar technologies.

transparent graphene [24]. This novel system can transition from a transparent state to a scattering state by heating, based on the phase transition between the smectic-A phase and the chiral nematic (i.e., CLC) phase; it effectively utilizes W-VO₂ to insulate infrared radiation. Yoon's group proposed a guest–host CLC system whose transmission can be changed by switching between the fingerprint (FP) and homeotropic (H) states [25]. The CLC doped with a black dye entails a low operating voltage.

In this study we incorporated a thermoresponsive chiral dopant (TCD) into a dual-frequency LC (DFLC) impregnated with a dichroic dye and a left-handed chiral dopant (S811). TCD exhibits right handedness at temperature T below ~ 50 °C, diminishing its right-handed chirality, becoming achiral, and possessing increasing left-handed chirality as T progressively rises. The two chiral dopants (TCD and S811) in a proper composition permit the system's chirality to be canceled out at low T , and as T is elevated, the overall (left-handed) chirality is substantially enhanced, enabling textural transformation from the transparent H state to the scattering FP state and, in turn, switching transmission. By adjusting the concentrations of chiral molecules, we can determine the temperature at which the optical texture changes, subsequently affecting the average transmission level. The average transmittance represents the mean transmission data within the wavelength range of 450–650 nm. We average the highest and lowest transmittance values from the T -rise curve in the transmittance–temperature plot and define the temperature at which the system reaches this level of transmittance as the switching temperature T_s . Additionally, applying a small alternating-current (AC) voltage at a frequency below the crossover frequency f_c sustains the H configuration to some extent, prompting the H–FP textural change to occur at an elevated T_s . Conversely, small applied voltage above f_c can lower T_s , thus greatly enhancing its tunability. Demanding only low power consumption, this approach overcomes the limitation of a fixed textural transition temperature in thermochromic smart windows and improves the selectivity of the active mode.

2. Experimental

2.1. Materials

To ascertain the helical twisting power (HTP) of either chiral dopant in the host at various T , we adopted the methodology proposed by Chang et al. [26] and prepared three samples (S1–S3) accordingly. This entailed the individual addition of the left-handed chiral dopant S811, the right-handed chiral dopant R5011, and the binary chiral mixture [27]—comprising the thermoresponsive chiral dopant TCD [28] and R5011—into the host DFLLC. TCD is a temperature-sensitive chiral agent that transitions from right-handed chirality to achirality (zero chirality) and then to left-handed chirality as the temperature increases. Its handedness is reversed at about 55 °C, exhibiting left-handedness at temperatures beyond 55 °C. The DFLLC HEF951800 (HCCH, China) exhibits dielectric anisotropy of 2.1 (measured at frequency f of 1 kHz and $T = 20$ °C), birefringence of 0.222 (at $\lambda = 589$ nm and $T = 25$ °C), and clearing point observed at 104 °C. Subsequently, these three mixtures were individually injected into commercial planar cells sourced from Chiptek (Miaoli, Taiwan) by capillary action. The consistent 6- μ m-thick cell gap, along with the polyimide (DL-3260, Nissan Chemical, Japan) coating configured in an antiparallel orientation, ensured the reliability and accuracy of our measurements. Leveraging the characterization data of the three CLC samples (denoted as S1, S2, and S3, respectively), we developed a thermoresponsive CLC with its composition specifically tailored for demonstration of smart-window applications by fabricating a handmade cell, S4. In the Results and discussion section, we will examine the properties of S4. The process of making the handmade cell is as follows: The commercial polyimide AL-8395D (Daily Polymer, Taiwan) was spin-coated on two indium–tin-oxide glass substrates. Then, the substrates underwent successive baking and unidirectional

rubbing to establish vertical alignment for the LC molecules. Following these processes, the assembled cell was securely fixed using AB glue mixed with rod spacers (10 μ m in diameter). Afterwards, the cell composed of two antiparallel rubbed substrates was filled by capillarity with a mixture of four components: the DFLLC, TCD, S811, and the dichroic dye S428 (Mitsui Chemical, Japan). Here the dichroic black dye was used to absorb the incident light to promote the contrast ratio. Further details regarding samples S1–S4 prepared for pretest (S1–S3) and focused investigation (S4) are presented in Table 1.

2.2. Measurement of optical properties

To assess the optical properties of the DFLLC host, we measured the refractive index of HEF951800 at various T ranging from 10 to 55 °C across five wavelengths (486 nm, 540 nm, 589 nm, 610 nm, and 680 nm). The measurement was conducted using a multi-wavelength Abbe refractometer (ATAGO DR-M4, accuracy of $\pm 2 \times 10^{-4}$) equipped with a recirculating cooling system (FIRSTEK B401L). In addition, to analyze transmittance across the spectral range of 380–780 nm, we employed a fiber-optic spectrometer (Ocean Optics HR2000+) coupled with a halogen light source (Ocean Optics HL2000). Haze was evaluated using a haze meter (Nippon Denshoku COH-5500). Optical texture observations were performed using a polarizing optical microscope (POM) fitted with two crossed linear polarizers (Olympus BX51-P). A function generator (Tektronix AFG-3022B) paired with a power amplifier (TREK 603) was exploited to generate square wave AC voltages at different f . To document transmission spectra and haze at each temperature, we maintained the samples within a temperature-controlled system (Linkam T95-PE), ensuring precise and consistent temperature conditions. All measurements of transmission and haze spectra were accomplished with unpolarized light.

2.3. Measurement of dielectric characteristics

To determine dielectric anisotropy across various f , the dielectric properties were analyzed utilizing a high-precision LCR meter (Keysight E4980A) with a 0.5-V_{rms} sinusoidal voltage probe in a frequency range spanning from 20 Hz to 2 MHz. The LCR meter was interfaced with a computer via a GPIB interface card, and data acquisition was executed by means of a LabVIEW graphical control program. All measurements were carried out in a temperature-controlled environment (Linkam T95-PE).

3. Design of the thermosensitive CLC

To design a smart window incorporating the chiral dopants S811 and TCD, it is crucial to determine HTP of each dopant in the nematic DFLLC host at various T . HTP, typically expressed in μm^{-1} , signifies positivity for right-handed chirality and negativity for left-handed chirality. The magnitude of this value is influenced by the material properties of the respective chiral dopant, as outlined in the following equation:

$$\frac{1}{|\text{HTP}| \cdot c} = p. \quad (1)$$

Both the magnitude of the HTP value and weight-percent concentration c of the chiral dopant significantly affect the pitch (length) p of CLC molecules in the Grandjean planar state. Moreover, considering

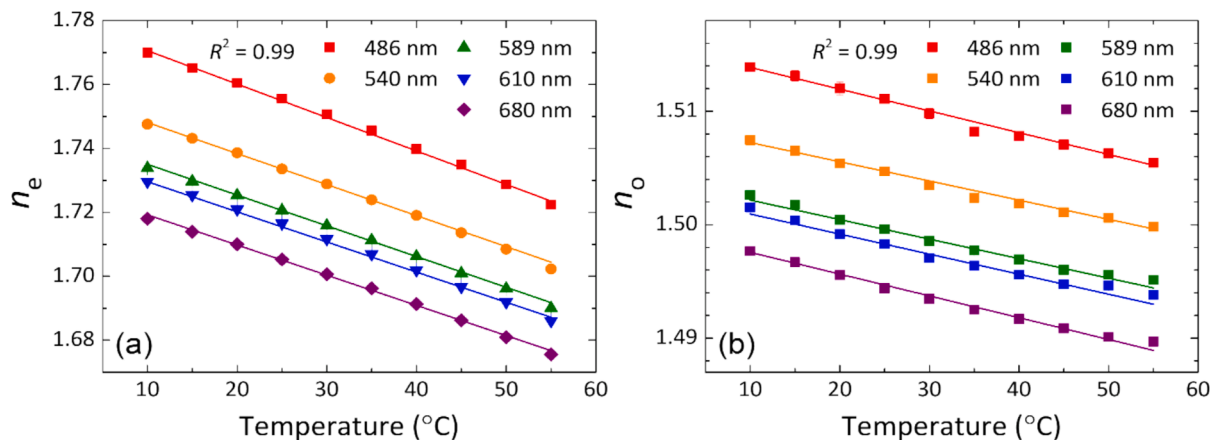
$$p = \lambda_c / \bar{n}, \quad (2)$$

one can determine p by the ratio of the central wavelength of the Bragg reflection band (λ_c) to the average (\bar{n}) of extraordinary and ordinary refractive indices (n_e and n_o , respectively) of the LC. By substituting Eq. (1) into Eq. (2), we can utilize λ_c , n_e , and n_o to calculate the approximate estimation of the T -dependent HTP value. Both n_e and n_o of DFLLC were measured at various T across diverse λ . Fig. 1 shows that both n_e and n_o

Table 1

The proportioning and conditions of four CLC samples.

Sample	Host	Alignment material	Chiral dopant	Chiral dopant concentration (wt.%)	Dye (S428) concentration (wt.%)	Cell gap (μm)
S1	HEF951800	DL-3260	S811	24.9	0	6.0
S2	HEF951800	DL-3260	R5011	2.5	0	6.0
S3	HEF951800	DL-3260	R5011/TCD	2.3/10.2	0	6.0
S4	HEF951800	AL-8395D	S811/TCD	1.9/10.0	1.0	9.7

**Fig. 1.** T -dependent refractive indices of the DFLC host HEF951800 at various λ : (a) extraordinary refractive index and (b) ordinary refractive index. R^2 in the legends is the coefficient of determination.

decrease linearly with increasing T at $\lambda = 486$ nm, 540 nm, 589 nm, 610 nm, and 680 nm, aligning with the mathematical expression [29]:

$$n(T) = n^0 - \alpha T, \quad (3)$$

where $n(T)$ represents the refractive index, n_e or n_o , as a function of T , and n^0 signifies the refractive index at absolute zero. The coefficient $-\alpha$ (in K^{-1}) indicates the slope of the fitted n - T curve. The fitted values of n^0 and α are presented in Table 2.

To further determine n_e and n_o at λ_c , we utilized the Cauchy dispersion equation [30]:

$$n(\lambda) = A + \frac{B}{\lambda^2} + \frac{C}{\lambda^4}, \quad (4)$$

where A , B , and C denote the Cauchy coefficients. The fitted curves at a given T allow the two indices of refraction to be acquired at an arbitrary wavelength. Fig. 2 reveals that both n_e and n_o of DFLC decrease monotonically with increasing λ at T of 20, 30, 40, and 50 $^\circ\text{C}$, following the Cauchy dispersion equation. The fitting coefficients A , B , and C of n_e and n_o values are listed in Table 3

Fig. 3(a), (b), and (c) shows the transmission spectra of CLC comprising 24.9-wt% S811 (S1), 2.50-wt% R5011 (S2), and a binary chiral mixture of 2.3-wt% R5011 and 10.2-wt% TCD (S3), respectively, at four representative T . From Fig. 3(a) and (b), it is observed that λ_c of S1 and S2 are around 550 nm and 630 nm, respectively, within the T range of 20–50 $^\circ\text{C}$. According to Eqs. (1) and (2), along with the Eq. (4), HTP of S811 in HEF951800 was calculated to be approximately $11.8 \mu\text{m}^{-1}$, as shown in Fig. 3(d), whereas that of R5011 is about $102 \mu\text{m}^{-1}$, as shown in Fig. 3(e). The variation in HTP of either chiral dopant with

varying T is minimal over the measurement range. On the other hand, since the HTP of TCD is too small to be measured independently, we thoughtfully introduced R5011 and ignored the intermolecular interaction between the two chiral compounds. Then p can be expressed as [31]

$$p = \frac{1}{[\text{HTP}_1 \cdot c_1 + \text{HTP}_2 \cdot c_2]}. \quad (5)$$

For the binary chiral mixture, the HTP of sole TCD can be calculated by substituting Eq. (1) into Eq. (5), namely, by utilizing R5011 to derive the HTP of TCD as a function of T . One can see from Fig. 3(c) that λ_c shifts from 581.3 to 612.4 nm as T rises from 20 to 50 $^\circ\text{C}$. Correspondingly, the HTP value of TCD in HEF951800 changes from $+1.76 \mu\text{m}^{-1}$ at 20 $^\circ\text{C}$ to $+0.41 \mu\text{m}^{-1}$ at 50 $^\circ\text{C}$ (Fig. 3(f)), suggesting that the right-handedness of TCD reduces and left-handedness escalates with elevated T . Notably, the pronounced staircase profile as shown in Fig. 3 (f) is a result of the CLC's compliance with imposed integer numbers of helical periods. Knowing the HTP values of S811 and TCD in HEF951800 at various T , we computationally determined the appropriate content of each chiral dopant for the preparation of thermosensitive CLC. The concentrations of S811 and TCD were set at 1.9 wt% and 10.0 wt%, respectively. By using the left-handed chiral dopant S811 and temperature-sensitive TCD in synergy, the torque is weakened at lower T , resulting in the CLC molecules in a vertical-alignment cell to be in the high-transmission H state. However, as T rises, the left-handed chirality of the material increases, leading to a reduction in p and transition to a low-transmission FP state. Deduced from Fig. 3(d) and (f), Fig. 4 illustrates the p value as a function of T calculated from 20 to 50 $^\circ\text{C}$.

Table 2

Fitting parameters of the refractive indices at 0 K of the DFLC in accordance with Eq. (3).

Refractive index	486 nm		540 nm		589 nm		610 nm		680 nm	
	n^0	α (10^{-4}K^{-1})								
n_e	1.781	10.5	1.758	9.70	1.745	9.60	1.739	9.40	1.729	9.44
n_o	1.516	1.92	1.509	1.69	1.504	1.72	1.503	1.77	1.500	1.92

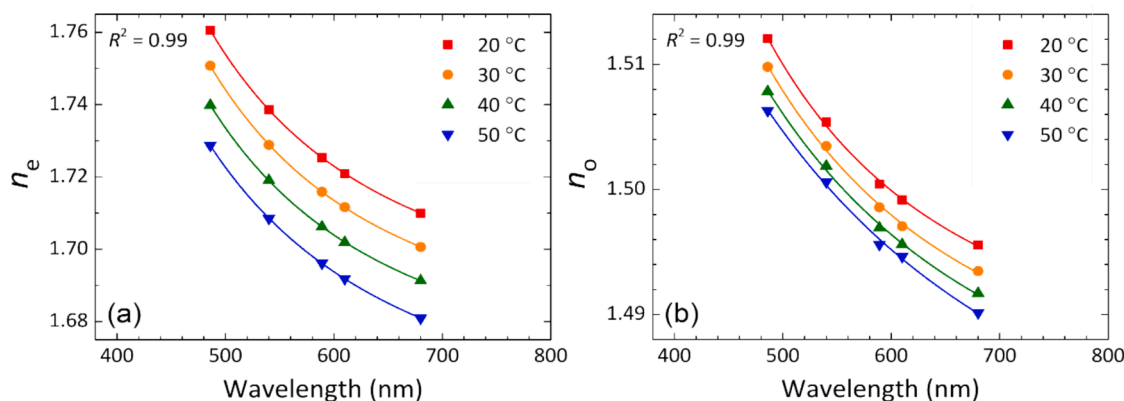


Fig. 2. λ -dependent refractive indices of the DFLC host HEF951800 at various T : (a) extraordinary refractive index and (b) ordinary refractive index. The symbols are experimental data and curves are fitted in accordance with Eq. (4).

Table 3

The fitting coefficients A , B , and C of the refractive indices of the DFLC in accordance with Eq. (4).

Temperature	A		B (μm^2)		C (μm^4)	
	A_e	A_o	B_e	B_o	C_e	C_o
20 °C	1.68	1.48	0.99	0.45	22.6	5.52
30 °C	1.67	1.48	0.97	0.59	22.6	3.28
40 °C	1.66	1.47	1.08	0.76	19.8	0.46
50 °C	1.65	1.47	1.33	0.97	19.2	-2.9

4. Results and discussion

Fig. 5 exemplifies three distinct passive-control switching mechanisms. The first showcases the reversible switching of the thermosensitive CLC between the transparent H state and opaque FP state without applied voltage ($V = 0$), as highlighted in Fig. 5(a), where the switching temperature T_s relies on the concentrations of S811 and TCD. Following the validation of the HTP behavior of chiral molecules as discussed in the preceding section, we meticulously tailored T_s to align with a representative temperature of 28 °C. Regarding the second working principle designated in the blue text in Fig. 5(b), a voltage operating at $f < f_c$ is administered to the CLC so that the reversible H–FP switching

takes place at a higher ambient temperature. The higher the voltage V , the higher the switching temperature T_s for textural transition. This outcome can be easily explained by the fact that applied voltage helps sustain the H configuration owing the CLC's positive dielectric anisotropy ($\Delta\epsilon > 0$). Conversely, the third case, highlighted in the red text in Fig. 5(b), operates in reverse. Application of voltage at a higher frequency ($f > f_c$) incites negative dielectric anisotropy ($\Delta\epsilon < 0$) in the CLC molecules, prompting them to tilt and subsequently reducing T_s . Analogous to the second mechanism, the extent of drop in T_s hinges on the magnitude of the applied voltage.

Optical texture serves as an effective method for observing the arrangement of LC molecules. The texture of the dye-doped CLC at various T is shown in Fig. 6(a). Below 25 °C, the optical texture exhibits slight localized light leakage in the H state due to some defects in conjunction with the residually weak left-handedness of the system at lower T , which hinders the uniformity of complete perpendicular orientation of CLC molecules to the glass substrate. Beyond 25 °C, the right-handedness of TCD subsides, leading to the formation of FP state. However, regions without light leakage under the POM remain visible on account of the insufficient HTP throughout the cell. Upon further increase in T to 35 °C, the p value decreases accordingly, allowing the CLC molecules to fully manifest in the FP configuration. Fig. 6(b) delineates the calculated thickness-to-pitch ratio (d/p) of the CLC system

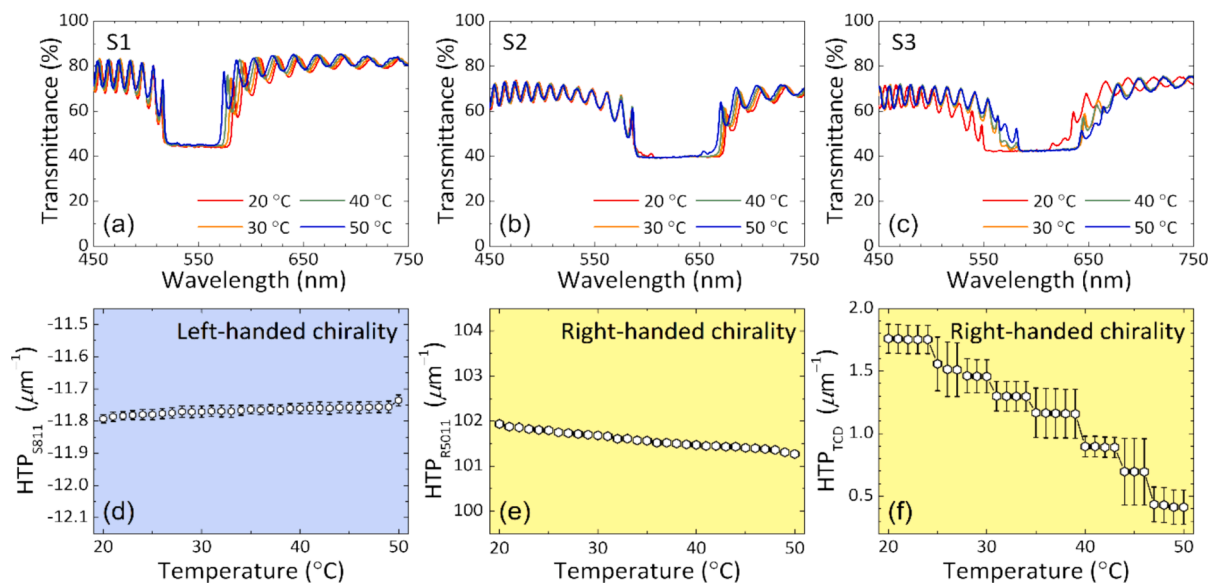


Fig. 3. Transmission spectra of the DFLC host HEF951800 doped with (a) 24.9 wt% of S811, (b) 2.5 wt% of R5011, and (c) R5011 at 2.3 wt% and TCD at 10.0 wt%, and T -dependent HTP of (d) S811, (e) R5011, and (f) TCD in HEF951800.

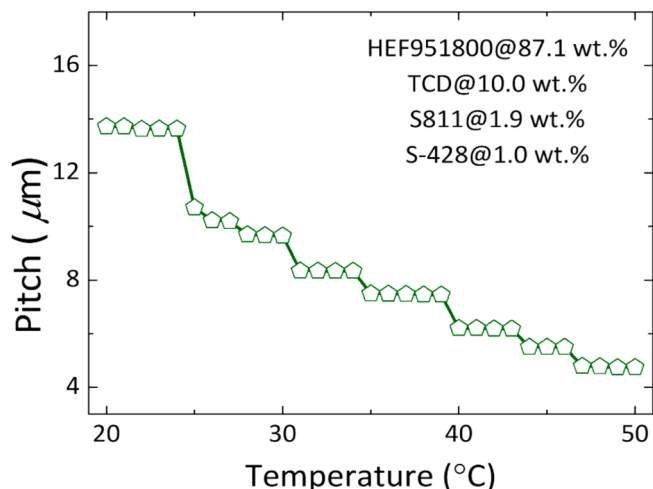


Fig. 4. T -dependent pitch of the dye-doped DFCLC system.

varying with temperature variations, corresponding to optical texture (Fig. 6(a)) in each of the three temperature regions. As d/p approaches approximately unity, FP texture begins to emerge. Various mixed states result when $1 \leq d/p < 1.5$. Fig. 6(c) illustrates the white-light transmittance and haze of the dye-doped system at the operating temperature. Transmission spectroscopy and haze measurements provide direct and valuable insights into the performance of optical components such as the one discussed in the study. In spectroscopic assessments conducted without the use of a polarizer, temperature control, either in a heating or cooling process, was adjusted at a rate of 1°C per minute. With a rise in T from 25 to 30°C , transmittance substantially falls from 74.0% to 19.3%, whereas haze increases from 5.1% to 33.9%. Fig. 6(d) demonstrates the reversibility-like nature of the chiral DFCL system. In consequence of the tendency of CLC molecules to take characteristics from the preceding configuration during texture switching, a temperature hysteresis (of $\sim 2^\circ\text{C}$) is observed between the heating and cooling curves. In the experiment, each spectrum was recorded at 1°C intervals. We have not thoroughly investigated the CLC device's performance at different heating/cooling rates because the time rate of 1°C per minute

seems sufficient for the sample to reach thermal equilibrium. Although the response time for switching between CLC configurations is not a major concern in a regular smart-window application, we speculate that the experimental hysteresis width can be reduced under lower-heating/cooling-rate conditions, say, 0.1°C per minute.

DFLC exhibits varying dielectric anisotropy at different T and f . To determine suitable f of applied voltage for a desired operation scheme in this study, we measured the parallel and vertical real-part dielectric permittivity (ϵ_{\parallel} and ϵ_{\perp} , respectively) of the dye-doped DFCLC in 10°C intervals, from 20 to 50°C . As illustrated in Fig. 7(a), the relaxation of ϵ_{\parallel} shifts to higher f with increasing T . To further analyze this phenomenon, we calculated $\Delta\epsilon$ in accordance with the definition

$$\Delta\epsilon \equiv \epsilon_{\parallel} - \epsilon_{\perp}. \quad (6)$$

The results are shown in Fig. 7(b), where the black horizontal dashed line specifies the f values at which $\Delta\epsilon = 0$ for the four different T . Additionally, the vertical dotted line instantiates a particular frequency of 30 kHz at which the DFCLC exhibits negative $\Delta\epsilon$ at 20°C and 30°C and yet positive $\Delta\epsilon$ at 40°C and 50°C . To lower T_s for textural switching between the H and FP states, one only needs to apply a fixed AC voltage operating at $f > f_c$ (28°C) ≈ 10 kHz, say, 30 kHz across the cell thickness. Likewise, one can utilize applied voltage at lower f , say, 1 kHz, to raise T_s , thereby adjusting the wanted temperature for textural switching.

As shown in Fig. 8(a) and (b), white-light transmission profiles of the dye-doped DFCLC subjected to AC voltages remain similar to that without the application of voltage, as depicted in Fig. 6(c). However, there is a significant difference in T_s . At null voltage, T_s of the sample is approximately 28°C (Fig. 6(c)). When a voltage of $3 V_{\text{rms}}$ at 1 kHz is applied, it generates an electric field that aligns the CLC molecules perpendicularly to the substrate plane. This voltage "stretches" p , reducing the d/p ratio and increasing T_s to 34°C . (The pitch can lengthen as the field increases until the helix is mostly composed of nematic-like regions oriented along the field.) Conversely, when a voltage of $2 V_{\text{rms}}$ at 30 kHz is applied, the CLC molecules tilt, weakening the strength of vertical alignment and causing T_s to drop to 22°C . Fig. 8 (c) and (d) illustrates the reversibility of the chiral material driving by a voltage. Note that, again, the tendency of LC molecules to keep their preceding texture brings about a temperature hysteresis (Fig. 6(d)).

The effect of continuous application of AC voltage on passive thermoregulation was investigated. Fig. 9(a) depicts white-light

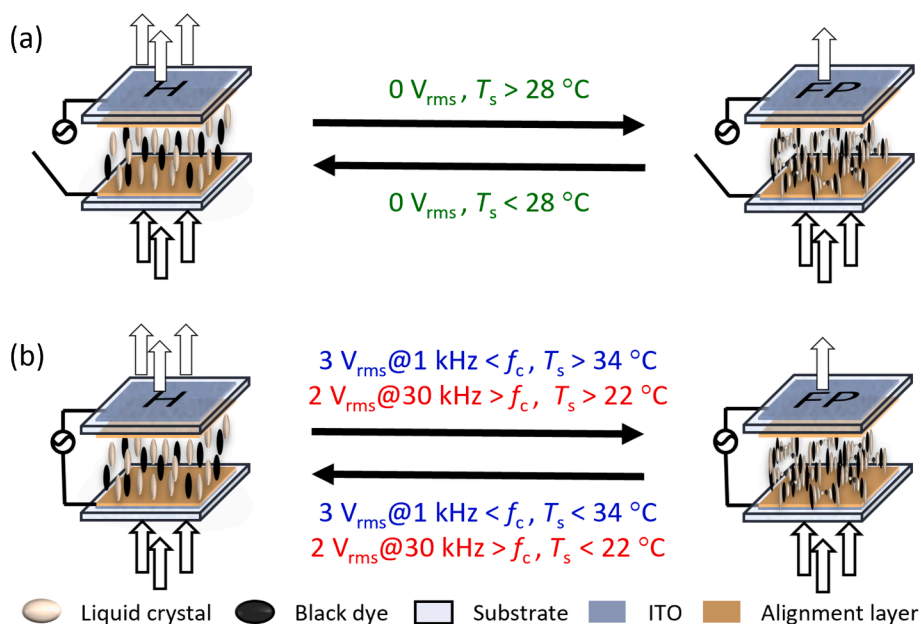


Fig. 5. Activation of textural transition in three passive-control modes by setting the desired voltage-controlled switching temperature: (a) without AC voltage and (b) with applied AC voltages at a higher and lower frequencies than the crossover frequency f_c .

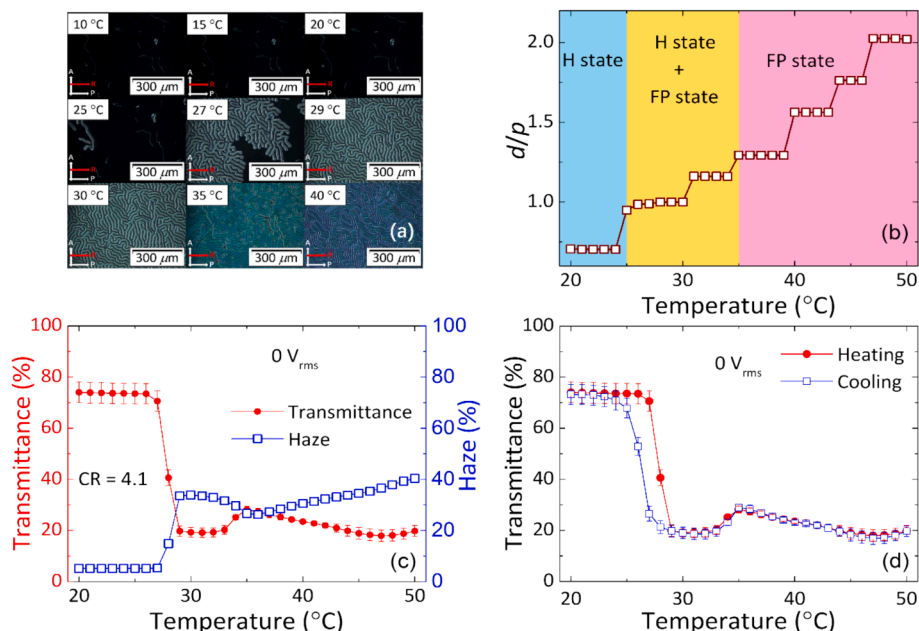


Fig. 6. (a) POM texture, (b) thickness-to-pitch ratio, (c) average transmittance and haze, and (d) reversibility examination of the dye-doped DFCLC cell conditioned at $0 V_{rms}$ in a range of temperatures between 20 and 50 °C. The contrast ratio, abbreviated as CR, is given in (c).

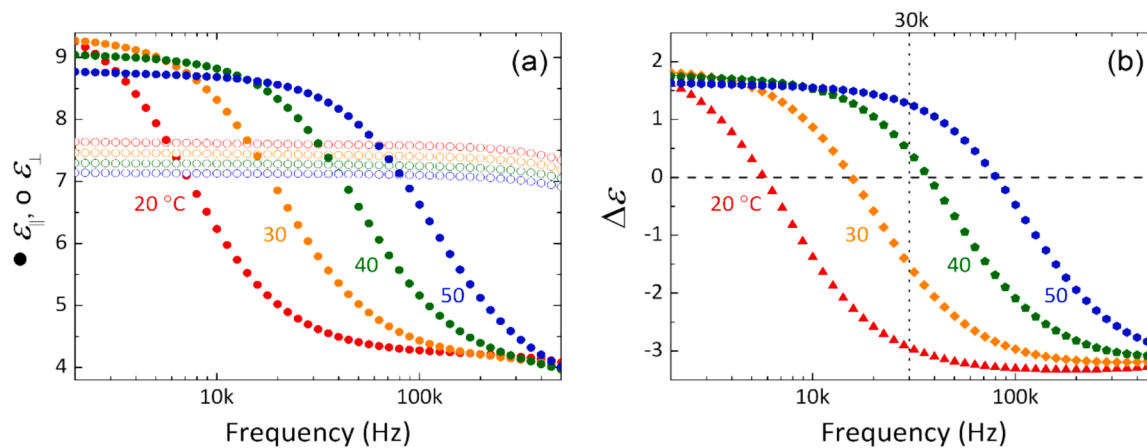


Fig. 7. (a) Parallel (filled symbols) and perpendicular (open symbols) components of the real-part dielectric spectra of thermosensitive dye-doped DFCLC at various T and (b) the corresponding curves of f -dependent dielectric anisotropy. Dielectric data of ϵ_{\parallel} and ϵ_{\perp} are acquired from vertical- and planar-alignment cells, respectively.

transmittance of the dye-doped DFCLC cell undergoing various voltages ranging from 0 to $8 V_{rms}$ at a lower frequency of 1 kHz. One can see from Fig. 9(a) that the transmission profiles are alike across all voltages, but, remarkably, T_s for texture transformation rises with increasing low- f voltage. When $8 V_{rms}$ is applied, the cell does not transition from the H state even at 45 °C because of the strong dielectric coupling. To demonstrate the functionality of voltage-adjustable T_s in the opposite direction to lower temperatures, which our previous effort is unable to achieve [26], Fig. 9(b) discloses T -dependent transmission at different voltages from 0 to $2.5 V_{rms}$ at 30 kHz. It can be seen that T_s decreases with increasing high- f voltage. Deduced from Fig. 9(a) and (b), respectively, Fig. 9(c) and (d) shows the interplay between applied voltage and switching temperature T_s . As mentioned in the Introduction section, T_s is defined as the temperature at which the dye-doped CLC cell reaches the transmission level of the average of the highest and lowest transmittance values from the transmittance–temperature plot obtained in the heating process. The two state diagrams facilitate prompt identification or prediction of the optical state—either the transparent H or opaque FP state—of the devised DFCLC cell in a given condition of known applied

voltage and ambient temperature. Note that translucent levels are possible around the border lines in Fig. 9(c) and (d).

In addition to the three passive controls discussed above, the cell empowers three active controls that elicit high, medium, and low transparency levels at $f < f_c$, $f > f_c$, and $f \approx f_c$, respectively. When a voltage is applied at a frequency $f < f_c$, the DFCLC molecules assume the H configuration, leading to highest transparency. Conversely, applying a voltage at $f > f_c$ gives rise to a translucent state. Depending on the applied voltage and the surrounding temperature, various degrees of translucency can be achieved. a uniform Grandjean planar (P) state can be obtained at a sufficiently high voltage. At $f = f_c$, the DFCLC molecules subjected to voltage encounter electrohydrodynamic instability, inducing a strong dynamic scattering (DS) state to render lowest transmission. These transparency levels are actively adjustable according to the user's preference. Fig. 10(a) illustrates the three states of the device under the active-control mode characterized by three dissimilar f , ranging from high to low transparency levels as shown from left to right. Displaying what were observed under a POM at 25 °C, Fig. 10(b) presents three optical textures induced by $10 V_{rms}$ operating at three

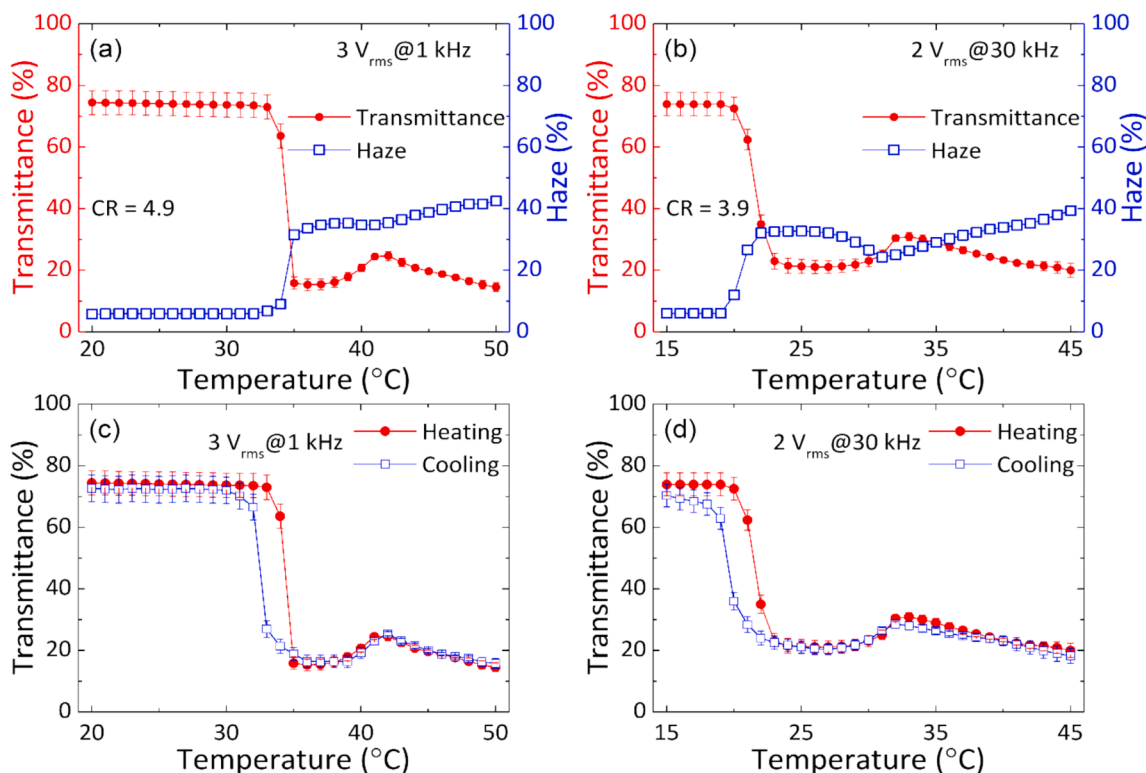


Fig. 8. T -dependent transmittance and haze of the dye-doped DFCLC cell at (a) $3 V_{rms}$, 1 kHz and (b) $2 V_{rms}$, 30 kHz and reversibility test at (c) $3 V_{rms}$, 1 kHz and (d) $2 V_{rms}$, 30 kHz. Given in both (a) and (b), the contrast ratio is abbreviated as CR.

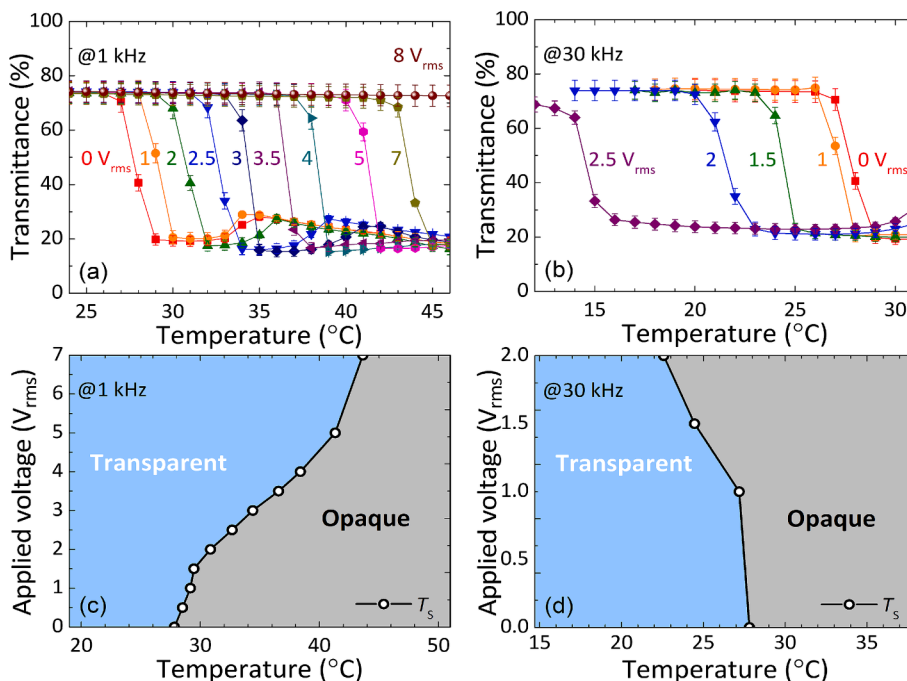


Fig. 9. Average transmittance as a function of T at various applied voltages in the ranges (a) from 0 to $8 V_{rms}$ at 1 kHz and (b) from 0 to $2.5 V_{rms}$ at 30 kHz; T -dependent applied AC voltage to impel the cell (c) from the opaque to transparent regime at 1 kHz and (d) from the transparent to opaque state at 30 kHz.

different f . In the case of $f = 30 \text{ kHz} > f_c (25^\circ\text{C})$, an incomplete P state (mixed with some FP texture) is generated by $10 V_{rms}$. Fig. 10(c) shows three photos of twin Einstein dolls positioned 75 cm behind the dye-doped DFCLC cell in the transparent, translucent, and opaque states. Unlike the case of the translucent state where light absorption is significant for the reduced transparency, minimal transparency in the

opaque state stems from optical DS in conjunction with absorption by the black dye. Due to the cell gap being $10 \mu\text{m}$ and the applied voltage being only as high as $10 V_{rms}$, the resulting small field strength (of $1 V_{rms} \cdot \mu\text{m}^{-1}$) does not induce observable dielectric heating. For the active mode, the switching time is of the order of 10 ms and it can be shortened to the millisecond scale with higher applied voltage. On the other hand,

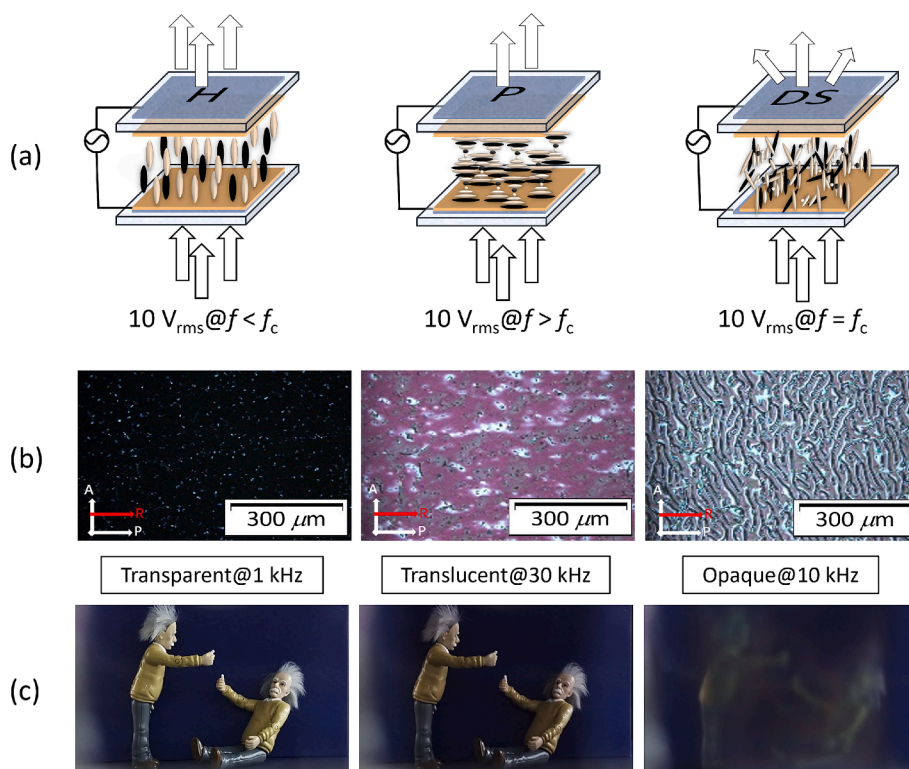


Fig. 10. (a) Schematic of CLC configurations in three different voltage-induced optical states, (b) POM textural micrographs obtained in the transmission mode at three designated frequencies, and (c) corresponding photographs of the same scene clarifying the electrically active control over the dye-doped cell driven by 10- V_{rms} voltage at 25 °C. P, A, and R in (b) represent the orientations of the transmission axes of the linear polarizer, analyzer, and rubbing direction. Photos in (c) were taken with a cell phone situated 5 cm in front of the dye-doped cell and the Albert Einstein dolls were right behind of the cell by a distance of 75 cm.

the response time is on the minute scale for the passive (or temperature-control) mode.

5. Conclusion

In conclusion, we have successfully demonstrated a DFCLC-based smart window with electrically tunable thermo-optical properties. By utilizing two chiral compounds and a dichroic dye, we fabricated a tunable guest–host thermosensitive CLC cell for smart window applications. The dye-doped DFCLC transitions from the high-transmission H state into low-transmission FP state as the d/p ratio approaches 1 in the heating process, achieving thermal responsiveness. Dielectric anisotropy in DFCLC allows us to overcome the limitation of fixed switching temperature T_s in a typical LC-based smart window. By adjusting different f within a 3- V_{rms} range, T_s can be tuned between 22 °C and 34 °C, making the device adaptable to various needs of a user or habitants living in specific climate zones. Additionally, applying various frequency ($f < f_c$, $f = f_c$, $f > f_c$) enables the system to switch between the transparent, translucent, and opaque states. Say, by adjusting f within a 10 V_{rms} , users can customize the window's transparency. With the novelty presented in this work, the DFCLC device features three passive and three active controls, offering more flexible and useful control options. This reported dual-mode smart window intriguingly unveils significant potential for practical applications.

Declaration of generative AI in scientific writing

ChatGPT (GPT-3.5, OpenAI's large-scale language-generation model) has been used to improve article readability and language.

CRediT authorship contribution statement

Zheng-Wei Lu: Writing – original draft, Visualization, Methodology, Investigation, Formal analysis, Data curation, Conceptualization. **Victor Ya. Zyryanov:** Validation, Conceptualization. **Wei Lee:** Writing – review & editing, Validation, Supervision, Resources, Project administration, Data curation, Conceptualization, Funding acquisition, Methodology, Visualization.

Declaration of competing interest

The authors declare that they have no known competing financial interests or personal relationships that could have appeared to influence the work reported in this paper.

Acknowledgments

Special thanks go to Yi-Cheng Chang (Global Research and Development Center, Taiwan Semiconductor Manufacturing Company) for conceptualization and methodology. This research was funded by the National Science and Technology Council, Taiwan (Nos. 111-2112-M-A49-033 and 112-2112-M-A49-031).

Data availability

Data will be made available on request.

References

- [1] G. Cai, A.L.S. Eh, L. Ji, P.S. Lee, Recent advances in electrochromic smart fenestration, *Adv. Sustain. Syst.* 1 (2017) 1700074.
- [2] A. Piccolo, F. Simone, Performance requirements for electrochromic smart window, *J. Build. Eng.* 3 (2015) 94–103.

- [3] X. Meng, S. Lin, S. Chen, X. Shen, D. Guo, J. Guo, Recent advances in smart windows based on photo-responsive liquid crystals featuring phase transition, *ChemPlusChem* (2024) e202300700.
- [4] W. Meng, A.J. Kragt, X. Hu, J.S. van der Burgt, A.P. Schenning, Y. Yue, G. Zhou, L. Li, P. Wei, W. Zhao, Photochromic thermoelectric smart window for season-adaptive solar heat and daylight management, *Adv. Funct. Mater.* (2024) 2402494.
- [5] M. Aburas, V. Soebarto, T. Williamson, R. Liang, H. Ebendorff-Heidepriem, Y. Wu, Thermochromic smart window technologies for building application: a review, *Appl. Energy* 255 (2019) 113522.
- [6] M. Kamalisarvestani, R. Saidur, S. Mekhilef, F. Javadi, Performance, materials and coating technologies of thermochromic thin films on smart windows, *Renew. Sustain. Energy* 26 (2013) 353–364.
- [7] S. Huang, Q. Zhang, P. Li, F. Ren, A. Yurtsever, D. Ma, High-performance suspended particle devices based on copper-reduced graphene oxide core-shell nanowire electrodes, *Adv. Energy Mater.* 8 (2018) 1703658.
- [8] A. Ghosh, B. Norton, A. Duffy, First outdoor characterisation of a PV powered suspended particle device switchable glazing, *Sol. Energy Mater.* 157 (2016) 1–9.
- [9] S. Leinberg, V. Kisand, A. Šutka, K. Saal, R. Löhmus, U. Joost, M. Timusk, E. Nõmmiste, Switchable optical transmittance of TiO₂ submicron-diameter wire suspension-based “smart window” device, *Opt. Mater. Express* 46 (2015) 418–422.
- [10] L. Jinqian, Y. Zhao, H. Gao, D. Wang, Z. Miao, H. Cao, Z. Yang, W. He, Polymer dispersed liquid crystals doped with CeO₂ nanoparticles for the smart window, *Liq. Cryst.* 49 (2022) 29–38.
- [11] W. Kamal, M. Li, J.D. Lin, E. Parry, Y. Jin, S.J. Elston, A.A. Castrejón-Pita, S. M. Morris, Spatially patterned polymer dispersed liquid crystals for image-integrated smart windows, *Adv. Opt. Mater.* 10 (2022) 2101748.
- [12] H. Zhang, Z. Miao, W. Shen, Development of polymer-dispersed liquid crystals: from mode innovation to applications, *Compos. - A: Appl. Sci. Manuf.* 163 (2022) 107234.
- [13] G. Cai, J. Wang, P.S. Lee, Next-generation multifunctional electrochromic devices, *Acc. Chem. Res.* 49 (2016) 1469–1476.
- [14] H. Zhang, J. Feng, F. Sun, D. Zhou, G. Cao, S. Wang, X. Hu, J. Ma, F. Su, Y. Tian, Self-driven Ni-based electrochromic devices for energy-efficient smart windows, *Adv. Mater. Technol.* 8 (2023) 2201688.
- [15] C.Y. Jeong, T. Kubota, K. Tajima, M. Kitamura, H. Imai, Complementary electrochromic devices based on acrylic substrates for smart window applications in aircrafts, *Mater. Chem. Phys.* 277 (2022) 125460.
- [16] L. Luo, Y. Liang, Y. Feng, D. Mo, Y. Zhang, J. Chen, Recent progress on preparation strategies of liquid crystal smart windows, *Crystal* 12 (2022) 1426.
- [17] B. Tylkowski, R. Jastrzab, M. Skrobańska, Photo-sensitive complexes based on azobenzene, *Sci. Rev.* 1 (2016) 20160002.
- [18] Y. Huang, H.K. Bisoyi, S. Huang, M. Wang, X.M. Chen, Z. Liu, H. Yang, Q. Li, Bioinspired synergistic photochromic luminescence and programmable liquid crystal actuators, *Angew. Chem. Int. Ed.* 60 (2021) 11247–11251.
- [19] M.J. Moran, M. Magrini, D.M. Walba, I. Aprahamian, Driving a liquid crystal phase transition using a photochromic hydrazone, *J. Am. Chem. Soc.* 140 (2018) 13623–13627.
- [20] W. Meng, Y. Gao, X. Hu, L. Tan, L. Li, G. Zhou, H. Yang, J. Wang, L. Jiang, Photothermal dual passively driven liquid crystal smart window, *ACS Appl. Mater. Interfaces* 14 (2022) 28301–28309.
- [21] S. Shaik, K. Gorantla, S. Mishra, K.S. Kulkarni, Thermal and cost assessment of various polymer-dispersed liquid crystal film smart windows for energy efficient buildings, *Constr. Build. Mater.* 263 (2020) 120155.
- [22] S.-M. Guo, X. Liang, C.-H. Zhang, M. Chen, C. Shen, L.-Y. Zhang, X. Yuan, B.-F. He, H. Yang, Preparation of a thermally light-transmittance-controllable film from a coexistent system of polymer-dispersed and polymer-stabilized liquid crystals, *ACS Appl. Mater. Interfaces* 9 (2017) 2942–2947.
- [23] X. Liang, C. Guo, M. Chen, S. Guo, L. Zhang, F. Li, S. Guo, H. Yang, A roll-to-roll process for multi-responsive soft-matter composite films containing Cs x WO₃ nanorods for energy-efficient smart window applications, *Nanoscale Horiz.* 2 (2017) 319–325.
- [24] X. Liang, M. Chen, Q. Wang, S. Guo, L. Zhang, H. Yang, Active and passive modulation of solar light transmittance in a hybrid thermochromic soft-matter system for energy-saving smart window applications, *J. Mater. Chem. C* 6 (2018) 7054–7062.
- [25] S.-W. Oh, S.-M. Ji, C.-H. Han, T.-H. Yoon, A cholesteric liquid crystal smart window with a low operating voltage, *Dyes Pigm.* 197 (2022) 109843.
- [26] Y.-C. Chang, S.-H. Yang, V.Y. Zyryanov, W. Lee, Electrically tunable thermoresponsive optic switch for smart window application based on dye-doped cholesteric liquid crystal, *J. Mol. Liq.* 388 (2023) 122752.
- [27] A.H. Gevorgyan, R.B. Alaverdyan, H. Gharagulyan, M.S. Rafayelyan, H. Grigoryan, Diffusion in liquid crystals of two cholesterics with different pitches, *J. Nanophotonics* 9 (1) (2015) 093591.
- [28] G. Heppke, D. Löttsch, F. Oestreicher, Esters of (S)-1, 2-propanediol and (R, R)-2, 3-butanediol—chiral compounds inducing cholesteric phases with a helix inversion, *Z. Naturforsch. A* 42 (1987) 279–283.
- [29] J. Li, G. Baird, Y.H. Lin, H. Ren, S.T. Wu, Refractive-index matching between liquid crystals and photopolymers, *J. Inf. Disp.* 13 (2005) 1017–1026.
- [30] P.-C. Wu, S. Kumar, W. Lee, Introduction: from conventional to unconventional liquid crystals, in: W. Lee, S. Kumar (Eds.), *Unconventional Liquid Crystals and Their Applications*, De Gruyter, Berlin, July 19, 2021, Chap. 1, pp. 1–108 (ISBN-10: 3110583038).
- [31] Y.-J. Liu, P.-C. Wu, W. Lee, Spectral variations in selective reflection in cholesteric liquid crystals containing opposite-handed chiral dopants, *Mol. Cryst. Liq. Cryst.* 596 (2014) 37–44.